JACS
JOURNAL OF THE AMERICAN CHEMICAL SOCIETY
Article
pubs.acs.org/JACS

Highly Emitting Near-Infrared Lanthanide "Encapsulated Sandwich" Metallacrown Complexes with Excitation Shifted Toward Lower Energy

Evan R. Trivedi,[†,‡] Svetlana V. Eliseeva,[§,∥,‡] Joseph Jankolovits,[†] Marilyn M. Olmstead,[⊥] Stéphane Petoud,*[,§] and Vincent L. Pecoraro*[,†]

[†]Department of Chemistry, Willard H. Dow Laboratories, University of Michigan, Ann Arbor, Michigan 48109, United States
[§]Centre de Biophysique Moléculaire, CNRS, UPR 4301, 45071 Orléans Cedex 2, France
[∥]Le STUDIUM® Loire Valley Institute for Advanced Studies, 1 Rue Dupanloup, 45000 Orléans, France
[⊥]Department of Chemistry, University of California, Davis, One Shields Avenue, Davis, California 95616, United States

Supporting Information

ABSTRACT: Near-infrared (NIR) luminescent lanthanide complexes hold great promise for practical applications, as their optical properties have several complementary advantages over organic fluorophores and semiconductor nanoparticles. The fundamental challenge for lanthanide luminescence is their sensitization through suitable chromophores. The use of the metallacrown (MC) motif is an innovative strategy to arrange several organic sensitizers at a well-controlled distance from a lanthanide cation. Herein we report a series of lanthanide "encapsulated sandwich" MC complexes of the form $Ln^{3+}[12\text{-}MC_{Zn(II),quinHA}\text{-}4]_2[24\text{-}MC_{Zn(II),quinHA}\text{-}8]$ ($\mathbf{Ln^{3+}[Zn(II)MC_{quinHA}]}$) in which the MC framework is formed by the self-assembly of Zn^{2+} ions and tetradentate chromophoric ligands based on quinaldichydroxamic acid (quinHA). A first-generation of luminescent MCs was presented previously but was limited due to excitation wavelengths in the UV. We report here that through the design of the chromophore of the MC assembly, we have significantly shifted the absorption wavelength toward lower energy (450 nm). In addition to this near-visible inter- and/or intraligand charge transfer absorption, $\mathbf{Ln^{3+}[Zn(II)MC_{quinHA}]}$ exhibits remarkably high quantum yields, long luminescence lifetimes (CD_3OD; Yb^{3+}, Q^L_{Ln} = 2.88(2)%, τ_{obs} = 150.7(2) μs; Nd^{3+}, Q^L_{Ln} = 1.35(1)%, τ_{obs} = 4.11(3) μs; Er^{3+}, Q^L_{Ln} = 3.60(6)·10^{-2}%, τ_{obs} = 11.40(3) μs), and excellent photostability. Quantum yields of Nd^{3+} and Er^{3+} MCs in the solid state and in deuterated solvents, upon excitation at low energy, are the highest values among NIR-emitting lanthanide complexes containing C−H bonds. The versatility of the MC strategy allows modifications in the excitation wavelength and absorptivity through the appropriate design of the ligand sensitizer, providing a highly efficient platform with tunable properties.

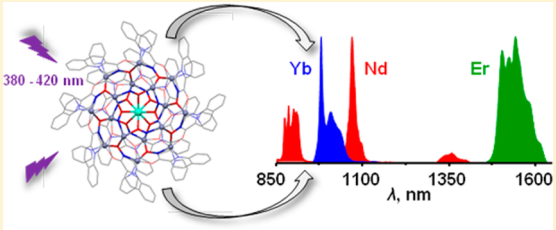

INTRODUCTION

The specificity of f-f emission signals and long luminescence lifetimes (μs-ms range)[1] have made lanthanide ions (Ln^{3+}) the key elements for a large number of novel advanced applications and technologies.[2−6] In particular, the ability of some lanthanide ions to exhibit characteristic sharp bands in the near-infrared (NIR) spectral region has stirred an additional interest for their exciting use in bioanalytical applications and biological imaging,[7−13] in telecommunications,[14,15] lasers, OLED/LED devices,[16] and energy conversion.[17,18] The Er^{3+} ion, with its emission band centered at 1530−1540 nm, is the best candidate for telecommunications. Biological optical imaging suffers from several negative effects caused by the interaction of light with biological media, thereby limiting the sensitivity of detection, penetration depth, and resolution. Among these limitations are autofluorescence, high absorption of hemoglobin in tissue in the visible range, and light scattering. As a consequence, NIR imaging and bioanalytical applications are gaining attention, and different luminescent probes have been developed.[19] With respect to the design of lanthanide-based luminescent materials, one must take into account the fact that most of the Ln^{3+} ion's f-f transitions are forbidden. Consequently, these transitions have low absorption coefficients, and direct population of excited states is only possible with the help of high-power laser excitation sources. However, one practical approach is a "sensitization" process also known as the "antenna effect" which involves embedding lanthanide ions into an environment (either an inorganic matrix or organic surroundings) with good light-harvesting properties. Captured excitation energy is then transferred to the lanthanide ion which, in turn, lights up with characteristic emission bands.[20] Different NIR luminescent lanthanide molecules and materials have been created based on mononuclear complexes with macrocyclic and acyclic ligands[21−23] and, more recently, nanoparticles,[24−26] dendrimers,[27−31] mesoporous solids,[32−34]

Received: November 13, 2013
Published: January 10, 2014

   dx.doi.org/10.1021/ja4113337 | J. Am. Chem. Soc. 2014, 136, 1526−1534

MOFs,[35−38] and 3d-4f heterometallic clusters.[39−43] Quantitative sensitization efficiencies can be achieved;[44] however, despite numerous efforts, the highest reported overall quantum yields for NIR-emitting lanthanide complexes containing C−H bonds are inferior: 3.8% for Yb^{3+}, 0.42% for Nd^{3+}, and 0.033% for Er^{3+}.[12,14,45] Such a large difference compared to visible-emitting lanthanide complexes, with quantum yields greater than 80% for Eu^{3+} and Tb^{3+},[46,47] can be explained as follows: small energy gaps between the emitting and first levels of the ground multiplet for NIR-emitting lanthanides are easily coupled to the overtone of high-energy oscillations, such as O−H, N−H, and C−H bonds. Such vibrations are often present in organic antennae.[48] An enhancement of luminescence efficiency can be achieved by deuteration[49,50] or halogenation[51−53] of organic ligands but requires significant synthetic effort.

One promising 3d-4f heterometallic platform that provides combined sensitization and protection of Ln^{3+} ions from vibrations is a class of supramolecular structures called metallacrowns (MCs). MCs have a repeating $[M-N-O]_n$ subunit and are named on the basis of their similarities to classical organic crown ethers, which contain a repeating $[C-C-O]_n$ subunit (Chart 1). A $[12\text{-}MC_{Zn(II),quinHA}\text{-}4]$ structure,

Chart 1

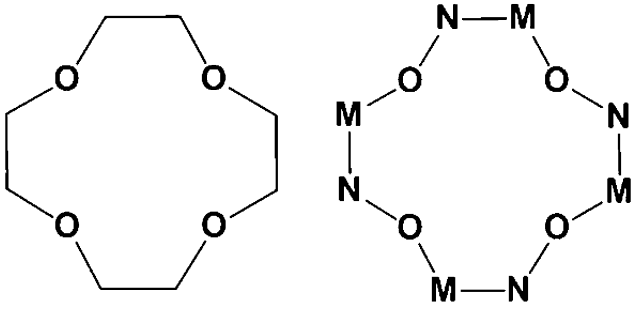

for example, contains a total of twelve atoms in the ring, four repeating units, Zn^{2+} as the ring metal, and quinaldichydroxamic acid (quinHA) as the organic ligand. In a similar manner to the classical crown ethers, a central metal atom can be bound to the inward facing oxygen atoms of the MC ring. Several MCs have been prepared with different sizes (e.g., 9-MC-3 to 60-MC-20) and bound metal ions.[54] Of particular interest with respect to luminescence properties are MCs that bind central lanthanide ions, of which there are several recent examples.[55−62] More specifically, Ln^{3+}[Zn(II)MC]s have been shown to exhibit NIR luminescence upon UV excitation through the chromophore located on the ligand.[63] In these structures, a single Ln^{3+} ion is sandwiched between two $[12\text{-}MC_{Zn(II),picHA}\text{-}4]$ structures (picHA = picolinehydroxamic acid). This "sandwich" is further encapsulated by a $[24\text{-}MC_{Zn(II),picHA}\text{-}8]$ structure. The resulting encapsulated motif, with the formula $Ln^{3+}[12\text{-}MC_{Zn(II),picHA}\text{-}4]_2[24\text{-}MC_{Zn(II),picHA}\text{-}8]$ ($\mathbf{Ln^{3+}[Zn(II)MC_{picHA}]}$), protects the Ln^{3+} ion from interactions with high energy X-H oscillators (X = N, O, C) nearby, preventing strong nonradiative deactivation, thereby enhancing the luminescence signal. However, UV absorption of this family of MCs limits the scope of practical applications, especially in the field of biological imaging. In order to shift excitation wavelength toward lower energy and to improve the sensitization efficiency, we report here the design, synthesis, and structural characterization of a series of second generation of MCs with the formula $Ln^{3+}[12\text{-}MC_{Zn(II),quinHA}\text{-}4]_2[24\text{-}MC_{Zn(II),quinHA}\text{-}8]$ ($\mathbf{Ln^{3+}[Zn(II)MC_{quinHA}]}$, quinHA = quinaldichydroxamic acid, Ln^{3+} = Y, Nd, Eu, Gd, Tb, Dy, Er, Yb) (Figure 1).

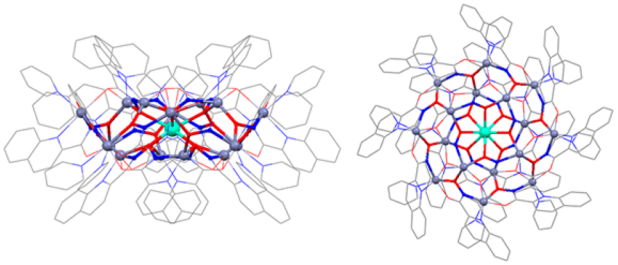

Figure 1. X-ray crystal structures of $\mathbf{Dy^{3+}[Zn(II)MC_{quinHA}]}$ viewed along the (**left**) *a*-axis and (**right**) *c*-axis.

Photophysical properties of NIR-emitting Nd^{3+}, Yb^{3+}, and Er^{3+} complexes have been investigated in detail. Additionally, in order to gather information about energy transfer processes, ligand-centered luminescence of $\mathbf{Gd^{3+}[Zn(II)MC_{quinHA}]}$ and quinHA are exploited.

EXPERIMENTAL SECTION

Quinaldichydroxamic Acid. Fresh hydroxylamine was prepared by combining hydroxylamine hydrochloride (12.0 g, 173 mmol) and potassium hydroxide (11.4 g, 173 mmol) in methanol (200 mL) at 0 °C. The solution was stirred for 20 min, filtered to remove potassium chloride, and set aside. Meanwhile, quinaldic acid (20.0 g, 116 mmol) and N-methylmorpholine (14.0 mL, 127 mmol) were combined with stirring in dichloromethane (300 mL). The solution was cooled to 0 °C at which time ethylchloroformate (12.1 mL, 127 mmol) was added. The reaction was stirred for 20 min and filtered, and the hydroxylamine solution was added to the filtrate at 0 °C. The reaction mixture was allowed to warm to room temperature and stirred for 1.5 h. The volume was reduced to ∼200 mL in vacuo, and water (1 L) was added to induce the precipitation of a white solid. The solid was collected by filtration and triturated with hot dichloromethane (800 mL) to yield quinaldichydroxamic acid (12.7 g, 58.2%) as a white powder. Mp 146−148 °C. ESI-MS, calc. for $[M + H^+]$, $C_{10}H_9N_2O_2$, 189.1; found 189.1; calc. for $[M + Na^+]$, $C_{10}H_8N_2NaO_2$, 211.0; found 211.1. ^{1}H NMR (400 MHz, DMSO-d_6) δ 11.51 (s, 1 H), 9.18 (s, 1 H), 8.53 (d, J = 8.5 Hz, 1 H), 8.09−8.04 (m, 3H),7.84 (m, 1 H), 7.69 (m, 1H). ^{13}C NMR (100 MHz, DMSO-d_6) δ 161.7, 150.3, 146.0, 137.6, 130.4, 129.2, 128.6, 128.0, 127.9, 118.7. Elem. Anal., calc. (found) for $(C_{10}H_8N_2O_2)(H_2O)$, C: 58.25 (58.25), H: 4.89 (4.94), N: 13.59 (13.65). UV−vis (MeOH), λ_{max}, nm (log ε) 207 (4.4), 238 (4.5), 300(br) (3.5).

Synthesis of $\mathbf{Dy^{3+}[Zn(II)MC_{quinHA}]}$. Quinaldichydroxamic acid (200 mg, 1.06 mmol), zinc triflate (385 mg, 1.06 mmol), and dysprosium triflate (81 mg, 0.13 mmol) were dissolved in 15 mL of dimethylformamide, and triethylamine (296 μL, 2.12 mmol) was added. The solution immediately turned yellow and was stirred at room temperature overnight at which time it was set aside for slow evaporation, producing yellow plate crystals within two weeks. Crystals were collected by filtration and air-dried to yield $\mathbf{Dy^{3+}[Zn(II)MC_{quinHA}]}$ as a triflate salt (29 mg, 8.4%). ESI-MS, calc. for $[M]^{3+}$, $C_{160}H_{96}DyN_{32}O_{32}Zn_{16}$, 1395.8; found 1395.7. Elem. Anal., calc. (found) for $(C_{163}H_{96}DyF_9N_{32}O_{41}S_3Zn_{16})(H_2O)_5(C_3H_7NO)_3$, C: 41.79 (41.81), H: 2.59 (2.81), N: 9.92 (10.23).

Y^{3+}[Zn(II)MC$_{quinHA}$]. (96 mg, 28%). ESI-MS, calc. for $[M]^{3+}$, $C_{160}H_{96}N_{32}O_{32}YZn_{16}$, 1371.1; found 1371.2. ^{1}H NMR (400 MHz, CD_3OD) δ 8.36 (d, J = 4.7 Hz, 8 H), 8.34 (d, J = 4.7 Hz, 8 H), 8.22 (d, J = 8.5 Hz, 8 H), 8.09 (d, J = 8.5 Hz, 8 H), 7.73 (d, J = 7.6 Hz, 8

dx.doi.org/10.1021/ja4113337 | J. Am. Chem. Soc. 2014, 136, 1526−1534

H), 7.52 (d, J = 8.5 Hz, 8 H), 7.49 (d, J = 8.0 Hz, 8 H), 7.25 (m, 16 H), 7.19 (d, J = 8.5 Hz, 8 H), 7.09 (m, 8 H), 6.95 (m, 8 H). Elem. Anal., calc. (found) for $(C_{163}H_{96}F_9N_{32}O_{41}S_3YZn_{16})(H_2O)_5(C_3H_7NO)_3$, C: 42.42 (42.48), H: 2.63 (2.90), N: 10.07 (10.40).

Yb^{3+}[Zn(II)MC$_{quinHA}$]. (96 mg, 28%). ESI-MS, calc. for $[M]^{3+}$, $C_{160}H_{96}N_{32}O_{32}YbZn_{16}$, 1399.3; found 1399.4. Elem. Anal., calc. (found) for $(C_{163}H_{96}F_9N_{32}O_{41}S_3YbZn_{16})(H_2O)_5(C_3H_7NO)_3$, C: 41.70 (41.73), H: 2.58 (2.74), N: 9.89 (9.98).

Nd^{3+}[Zn(II)MC$_{quinHA}$]. (58 mg, 34%). ESI-MS, calc. for $[M]^{3+}$, $C_{160}H_{96}N_{32}NdO_{32}Zn_{16}$, 1389.7; found 1389.2. Elem. Anal., calc. (found) for $(C_{163}H_{96}F_9N_{32}NdO_{41}S_3Zn_{16})(H_2O)_5(C_3H_7NO)_3$, C: 41.94 (41.76), H: 2.60 (2.76), N: 9.95 (10.08).

Gd^{3+}[Zn(II)MC$_{quinHA}$]. (67 mg, 39%). ESI-MS, calc. for $[M]^{3+}$, $C_{160}H_{96}GdN_{32}O_{32}Zn_{16}$, 1394.0; found 1393.2. Elem. Anal., calc. (found) for $(C_{163}H_{96}F_9GdN_{32}O_{41}S_3Zn_{16})(H_2O)_4(C_3H_7NO)_4$, C: 42.09 (41.84), H: 2.66 (3.03), N: 10.10 (10.26).

Tb^{3+}[Zn(II)MC$_{quinHA}$]. (39 mg, 23%) ESI-MS, calc. for $[M]^{3+}$, $C_{160}H_{96}N_{32}O_{32}TbZn_{16}$, 1394.5; found 1394.1. Elem. Anal., calc. (found) for $(C_{163}H_{96}F_9N_{32}O_{41}S_3TbZn_{16})(H_2O)_5(C_3H_7NO)_3$, C: 41.82 (41.50), H: 2.59 (2.71), N: 9.92 (9.90).

Eu^{3+}[Zn(II)MC$_{quinHA}$]. (69 mg, 40%). ESI-MS, calc. for $[M]^{3+}$, $C_{160}H_{96}EuN_{32}O_{32}Zn_{16}$, 1392.2; found 1391.8. Elem. Anal., calc. (found) for $(C_{163}H_{96}EuF_9N_{32}O_{41}S_3Zn_{16})(H_2O)_9(C_3H_7NO)_3$, C: 41.27 (41.00), H: 2.72 (2.90), N: 9.79 (9.80).

Er^{3+}[Zn(II)MC$_{quinHA}$]. (35 mg, 20%). ESI-MS, calc. for $[M]^{3+}$, $C_{160}H_{96}ErN_{32}O_{32}Zn_{16}$, 1397.3; found 1397.1. Elem. Anal., calc. (found) for $(C_{163}H_{96}ErF_9N_{32}O_{41}S_3Zn_{16})(H_2O)_5(C_3H_7NO)_3$, C: 41.15 (41.49), H: 2.71 (2.86), N: 9.76 (10.16).

Crystal Structure Determination of Dy^{3+}[Zn(II)MC$_{quinHA}$] ([DyZn$_{16}$(quinHA)$_{16}$(py)$_8$](CF$_3$SO$_3$)$_3$•2EtOAc). Yellow block crystals of **Dy^{3+}[Zn(II)MC$_{quinHA}$]** suitable for X-ray analysis were grown by slow diffusion of ethyl acetate into a DMF:pyridine (2:1, v:v) solution of the triflate salt. A crystal of dimensions 0.22 × 0.22 × 0.28 mm was selected for data collection and mounted in the 90 K nitrogen cold stream provided by a Cryosystems low temperature apparatus on the goniometer head of a Bruker D8 diffractometer equipped with an ApexII CCD detector. Data were collected with the use of Mo Kα radiation (λ = 0.71073 Å). The structure was solved by a dual space method (SHELXT) and refined by full-matrix least-squares on F^2 (SHELXL-2012). The molecule crystallized in the tetragonal crystal system, space group $P4$ (No. 75). It was refined as a two-component inversion twin. The occupancy of disordered triflate anions was restrained to meet charge balance. Further details of the crystal structure refinement are available in the Supporting Information.

Crystal data: $[C_{200}H_{136}DyN_{40}O_{32}Zn_{16}][CF_3SO_3]_3$•2($C_4H_8O_2$), fw = 5443.32, tetragonal, $P4$ (No. 75), a = 30.4975(19) Å, c = 13.3192(9) Å, V = 12388.2(18) Å^3, Z = 2, $R1$ [33073 reflections with $I > 2\sigma(I)$] = 0.0415, $wR2$ (all 37814 data) = 0.1402, 1506 parameters, 2 restraints.

Photophysical Measurements. Luminescence data were collected on samples placed into 2.4 mm i.d. quartz capillaries or quartz Suprasil cells. Emission and excitation spectra were measured on a Horiba-Jobin-YvonFluorolog 3 spectrofluorimeter equipped with either a visible photomultiplier tube (PMT) (220−800 nm, R928P; Hamamatsu), a NIR solid-state InGaAs detector cooled to 77 K (800−1600 nm, DSS-IGA020L; Jobin-Yvon), or NIR PMTs (950−1450 nm, H10330-45; 950−1650 nm, H10330-75; Hamamatsu). All spectra were corrected for instrumental functions. Luminescence lifetimes were determined under excitation at 355 nm provided by a Nd:YAG laser (YG 980; Quantel), while the signal was detected in the NIR by the aforementioned PMT (H10330-75). The output signal from the detectors was then fed to a 500 MHz bandpass digital oscilloscope (TDS 754C; Tektronix) and then transferred to a PC for treatment with Origin 8. Luminescence lifetimes are averages of at least three independent measurements. Quantum yields in the NIR were determined with a Fluorolog 3 spectrofluorimeter according to an absolute method using an integration sphere (GMP SA). Each sample was measured several times under slightly different experimental conditions. Estimated experimental error for quantum yields determination is 10%.

RESULTS AND DISCUSSION

Synthesis and Structural Characterization of Ln^{3+}[Zn(II)MC$_{quinHA}$]. The organic framework for these MC structures is based on quinaldichydroxamic acid (quinHA), which was prepared in one step from commercially available starting materials through an anhydride intermediate.[64] This synthesis proceeded in moderate yield (58%) but proved less tedious than direct esterification[65,66] or solid-phase methods.[67] The complete deprotonation of quinHA resulted in the formation of a tetradentate dianionic ligand whose charge complements Zn^{2+} in MC assembly. The reaction of quinHA with zinc(II) triflate, a lanthanide(III) triflate, and triethylamine (TEA) in dimethylformamide (DMF) produced a MC of the form $Ln^{3+}[12\text{-}MC_{Zn(II),quinHA}\text{-}4]_2[24\text{-}MC_{Zn(II),quinHA}\text{-}8](OTf)_3(DMF)_{8-x}(H_2O)_x$, where the lanthanide ion is sandwiched between two [12-MC$_{Zn(II),quinHA}$-4] and further encapsulated by a [24-MC$_{Zn(II),quinHA}$-8] (Scheme 1). A highly

Scheme 1. Ln^{3+}[Zn(II)MC$_{quinHA}$] Synthesis[a]

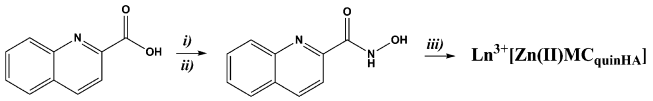

[a] *i)* *N*-methylmorpholine, ethylchloroformate, 0 °C, 20 min; *ii)* NH_2OH, 0 °C, 1.5 h; *iii)* 1 eq $Zn(OTf)_2$, 0.13 eq $Ln(OTf)_3$, 2 eq TEA, DMF, 19 °C, 24 h (OTf = triflate; Ln^{3+} = Dy^{3+}, Er^{3+}, Eu^{3+}, Gd^{3+}, Nd^{3+}, Tb^{3+}, Y^{3+}, Yb^{3+}).

pure product was crystallized by slow evaporation of the solvent and isolated as thin yellow plates. These crystals were, however, of insufficient quality for X-ray diffraction; an alternative crystallization method was developed for crystal structure determination, as discussed below. A relatively modest paramagnetic shift was observed in ^{1}H NMR spectra (Y^{3+} vs Eu^{3+}) (Figures S1 and S2), indicating that the protons of the ligand are sufficiently sequestered from interaction with the Ln^{3+} ion. This result is qualitative evidence that the Ln^{3+} ion is far enough from neighboring high energy C−H oscillators that would quench lanthanide luminescence. It was expected that the MC structure would contain eight solvent molecules coordinated to Zn^{2+} atoms of the [24-MC$_{Zn(II),quinHA}$-8]. ^{1}H NMR data (Ln = Y^{3+}, Yb^{3+}, Eu^{3+}) confirmed the presence of approximately three DMF per MC and an excess of water molecules; therefore, we assumed that five water molecules are coordinated to the Zn^{2+} metal ions. The addition of this number of solvent molecules to the calculated chemical composition produced an excellent match to experimental CHN elemental analyses.

Yellow block crystals of **Dy^{3+}[Zn(II)MC$_{quinHA}$]** suitable for X-ray analysis were grown by slow diffusion of ethyl acetate into a DMF:pyridine (2:1, v:v) solution of the triflate salt. The obtained asymmetric unit contains two independent one-quarter cations of $[Dy[12\text{-}MC_{Zn(II),quinHA}\text{-}4]_2[24\text{-}MC_{Zn(II),quinHA}\text{-}8](py)_8]^{3+}$, with the crystallographic 4-fold axis passing through the Dy^{3+} ions. The cation has overall 4-fold (S_8) symmetry (Figure 1) and can be considered to consist of three layers: a large radius [24-MC$_{Zn(II),quinHA}$-8](py)$_8$ ring (Figure 2a) sandwiched between two smaller concave [12-MC$_{Zn(II),quinHA}$-4] rings (Figure 2b). Figure 2a indicates the alternating bridging that connects the central metallacrown to the two outer ones. The interior Dy^{3+} ion is bonded to four hydroximate oxygens of each of the outer two metallacrowns,

dx.doi.org/10.1021/ja4113337 | J. Am. Chem. Soc. 2014, 136, 1526−1534

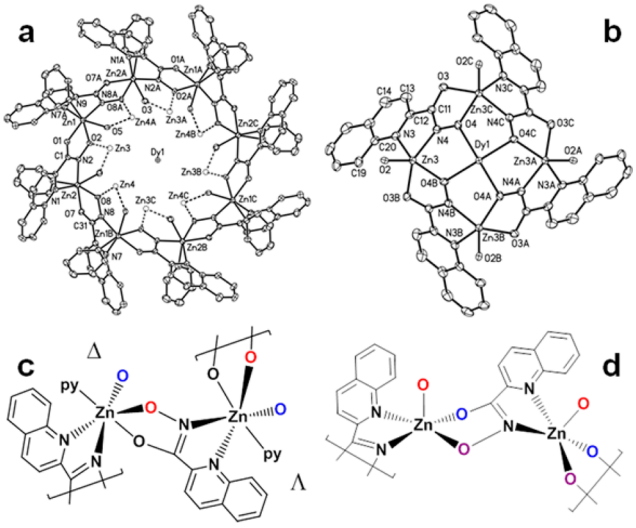

Figure 2. The three layers of $Dy^{3+}[Zn(II)MC_{quinHA}]$ are shown with 50% thermal displacement parameters and a partial numbering scheme. (**a**) Depiction of the central large crown, [24-$MC_{Zn(II),quinHA}$-8](py)$_8$, and the position of the nonbonded central Dy^{3+}. The dashed lines indicate how the central crown bridges to the smaller, capping, concave crowns. (**b**) One of the capping crowns of [12-$MC_{Zn(II),quinHA}$-4] as well as the coordination to Dy^{3+}. Coordination geometry of Zn^{2+} in the (**c**) [24-$MC_{Zn(II),quinHA}$-8] and (**d**) [12-$MC_{Zn(II),quinHA}$-4] structures indicates that the two distinct MC rings are linked through the [12-$MC_{Zn(II),quinHA}$-4] carboxylate oxygen (**blue**) and the [24-$MC_{Zn(II),quinHA}$-8] hydroximate oxygen (**red**) atoms. The Ln^{3+} ion is bound to the [12-$MC_{Zn(II),quinHA}$-4] hydroximate oxygen atoms (**purple**).

giving it an overall square antiprismatic coordination geometry. The coordination geometry of the Zn^{2+} ions varies between the [12-$MC_{Zn(II),quinHA}$-4] and [24-$MC_{Zn(II),quinHA}$-8], demonstrating a structural flexibility of Zn^{2+} that we intended to take advantage of. The Zn^{2+} ions in the [12-$MC_{Zn(II),quinHA}$-4] moieties have a distorted square pyramidal geometry, and the hydroximate oxygen atoms are coordinated to the Dy^{3+} ion (Figure 2d). The Zn^{2+} ions in the [24-$MC_{Zn(II),quinHA}$-8] moiety, however, are octahedral with alternating Δ/Λ absolute stereochemistry and one coordinated pyridine solvent molecule (Figure 2c). The two types of MC structures are linked together by the carbonyl and hydroximate oxygen atoms of [12-$MC_{Zn(II),quinHA}$-4] and [24-$MC_{Zn(II),quinHA}$-8], respectively, as indicated by the color scheme depicted in Figure 2c-d. Comparison of this structure to the previously reported [Tb[12-$MC_{Zn(II),picHA}$-4]$_2$[24-$MC_{Zn(II),picHA}$-8](py)$_8$]$^{3+}$ and [Dy-[12-$MC_{Zn(II),picHA}$-4]$_2$[24-$MC_{Zn(II),picHA}$-8](py)$_8$]$^{3+}$ reveals no significant deviation in coordination geometry around the Ln^{3+} ion. This evidence proves our assertion that a change in ligand has no effect on the Ln^{3+} ion's first coordination sphere, thereby presenting a platform with tunable absorptivity through the choice of organic chromophore.

High energy X−H oscillators (X = C, N, O) are a major source of vibrational deactivation of lanthanide luminescence. Therefore, an important parameter to be gleaned from the crystal structure data is the shortest Dy−CH distance, which was found to be 7.0 Å. This value represents an improvement over our previously reported complexes by 0.3 Å (ca. 4%). An apparent π-stacking interaction between the organic moieties of the [12-$MC_{Zn(II),quinHA}$-4] and [24-$MC_{Zn(II),quinHA}$-8] was observed. Adjacent quinoline rings are located ca. 4 Å apart with an alignment that deviates slightly from ideal parallelism (ca. 14°). This short distance opens the possibility for intramolecular through-space Inter- or Intra Ligand Charge Transfer (ILCT) transitions discussed below.

Photophysical Properties. The ligand quinHA exhibits several absorption bands in the UV region with apparent maxima centered at 238 and ≈300 nm resulting from $\pi^* \leftarrow \pi$ transitions located on the quinoline moiety; the long wavelength absorption trails to 340 nm (Figure 3). Upon

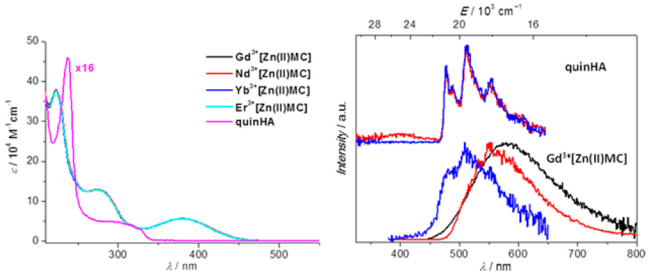

Figure 3. (**Left**) Absorption spectra of $Ln^{3+}[Zn(II)MC_{quinHA}]$ complexes (2.04×10^{-5} M, Ln^{3+} = Gd, Nd, Yb, Er) and quinHA (2.42×10^{-4} M) in methanol at 298 K. For the sake of comparison absorption spectrum of quinHA is multiplied by 16 times. (**Right**) Luminescence spectra of $Gd^{3+}[Zn(II)MC_{quinHA}]$ (λ_{ex} = 340 nm) and quinHA (λ_{ex} = 290 nm) at 298 K (**black**), at 77 K without delay (**red**) and with 100 μs delay after the excitation flash (**blue**).

deprotonation and formation of the $Ln^{3+}[Zn(II)MC_{quinHA}]$ framework, a blue shift of ≈15 nm is observed. In addition, a new broad absorption band appears in the near-visible region with an apparent maximum at 380 nm ($\varepsilon \approx 5.5 \times 10^4$ M^{-1} cm^{-1}) and extends to 470 nm. This band accounts for the yellow color of $Ln^{3+}[Zn(II)MC_{quinHA}]$ in both solid state and in solution. To ensure that this near-visible absorption band was not due to the electronic structure of the deprotonated ligand alone, quinHA was exposed to several equivalents of TEA and the absorption spectra remained unchanged (Figure S4). Therefore, one can reasonably assume, given that discrete Zn^{2+}complexes typically do not participate in either metal-to-ligand charge transfer (MLCT) or ligand-to-metal charge transfer (LMCT) transitions and absorption spectra are independent of the choice of the Ln^{3+} ion, that the near-visible band can be attributed to the presence of an ILCT state located at lower energy and caused by ligand charge redistribution which is unique to the quinHA ligand. A near-visible Zn^{2+} LMCT ($4s \leftarrow \pi$) transition has been observed for bulk semiconductor ZnO and ZnO colloidal crystals at ca. 365 nm;[68,69] however, we would expect this transition to occur at much higher energy for the complexes being discussed here.[70] In the case of $Yb^{3+}[Zn(II)MC_{quinHA}]$, a broad and very weak (ε ~5−7 M^{-1} cm^{-1}) band in the range 910−1000 nm assigned to an f-f absorption ($^2F_{5/2} \leftarrow {}^2F_{7/2}$) was detected (Figure S5).

The energy gap between ground and excited states for Gd^{3+} is very high in energy, and, therefore, it is impossible for the Gd^{3+} ion in the corresponding MCs to be sensitized through energy transfer from the ligand triplet/ILCT states. This characteristic can be used to our advantage to determine the energy levels of the MC complexes in the absence of energy transfer to the Ln^{3+} ion (but with the electronic state of the sensitizer being exposed to the electron deficient lanthanide cations). $Gd^{3+}[Zn(II)MC_{quinHA}]$ was exposed to UV excitation through the ILCT band at 340 nm at room temperature

dx.doi.org/10.1021/ja4113337 | J. Am. Chem. Soc. 2014, 136, 1526−1534

(Figure 3). We observed a weak broad-band emission with an apparent maximum located at 580−590 nm. The position of this band is insensitive to the excitation wavelength which was varied from 290 to 380 nm indicating that the energy is following the same path independently of the excitation wavelength. Lowering the temperature to 77 K led to a slight sharpening of the band and a shift of the maximum to an apparent maximum localized between 545 and 555 nm. A further blue shift toward 510 nm was observed upon application of a time delay of 100 μs after the excitation flash. This observation is rather unusual because, in general, one would expect a significant red shift of the phosphorescence band compared to the fluorescence band. Thus, we can hypothesize that the broad-band green emission of the $\mathbf{Gd^{3+}[Zn(II)MC_{quinHA}]}$ might be arising from a charge-transfer state, while emission from the singlet state (fluorescence) is quenched by self-absorption. In order to monitor the position of the triplet state in the absence of an ILCT state, we investigated emission properties of the ligand quinHA alone. Upon UV excitation at 290 nm at room temperature, quinHA does not display any detectable emission. At 77 K, a strong green luminescence band centered at 510 nm and a weaker intensity band in the 325−460 nm range can be observed. The latter band disappears upon enforcing a delay of 100 μs after the flash so it can be assigned to short-lived fluorescence, while the green emission is phosphorescence originating from the triplet state. The electronic envelope and vibrational splitting of the phosphorescence spectra of the $\mathbf{Gd^{3+}[Zn(II)MC_{quinHA}]}$ and the quinHA are nearly identical. Therefore, the energy of the triplet state of the ligand, determined from the 0−0 transition, is estimated to be located between 20 920 and 21 000 cm^{-1} (476−478 nm). The position of the lowest excited singlet and the ILCT states were determined from the intersection of the absorption and emission (fluorescence) spectra of quinHA and $\mathbf{Gd^{3+}[Zn(II)MC_{quinHA}]}$, respectively, and found to be located at 29 850 cm^{-1} (335 nm) and 21 560 cm^{-1} (464 nm). A proposed schematic diagram of the ligand's energy levels with respect to those of Yb^{3+}, Nd^{3+}, and Er^{3+} ions and possible energy migration paths are sketched in Figure 4. An appearance of the ILCT state allows shifting excitation toward longer wavelengths; moreover, ILCT states are known to participate in sensitization of lanthanide luminescence.[71] However, it should be noted that the energies of the ILCT and the triplet states are very similar in the investigated compounds, which can create additional ways for dissipation of the excitation energy through energy resonance.

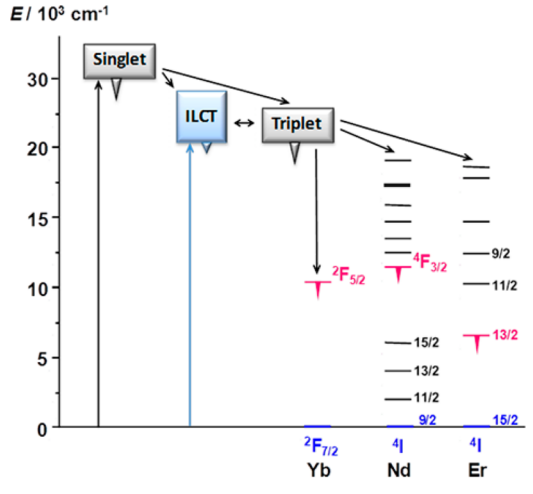

Figure 4. Schematic energy diagram showing the ligand and the lanthanides energy levels.

Luminescence spectra were recorded for $\mathbf{Ln^{3+}[Zn(II)MC_{quinHA}]}$complexes ($Ln^{3+}$ = Yb^{3+}, Nd^{3+}, Er^{3+}) in the solid state and in solution (CH_3OH/CD_3OD) using 370−420 nm photons as excitation. Complexes of the visible emitting Ln^{3+} ions (Ln^{3+} = Dy^{3+}, Eu^{3+}, Tb^{3+}) did not display any detectable lanthanide-based luminescence, which might be attributed to an insufficient sensitization due to closed positions of the ligand and Ln^{3+} energy levels in case of Dy^{3+} ($^4F_{9/2}$, 21 100 cm^{-1}) and Tb^{3+} ($^5D_4$, 20 500 cm^{-1}) or a presence of an additional nonradiative deactivation pathway through ligand-to-metal charge transfer states for Eu^{3+}. The NIR emitting MCs exhibit intense lanthanide characteristic emission arising from the $^2F_{5/2}\rightarrow{}^2F_{7/2}$, $^4F_{3/2}\rightarrow{}^4I_J$ (J = 9/2, 11/2, 13/2), and $^4I_{13/2}\rightarrow{}^4I_{15/2}$ transitions for the Yb^{3+}, Nd^{3+}, and Er^{3+} compounds, respectively (Figure 5). Excitation spectra of all studied MCs

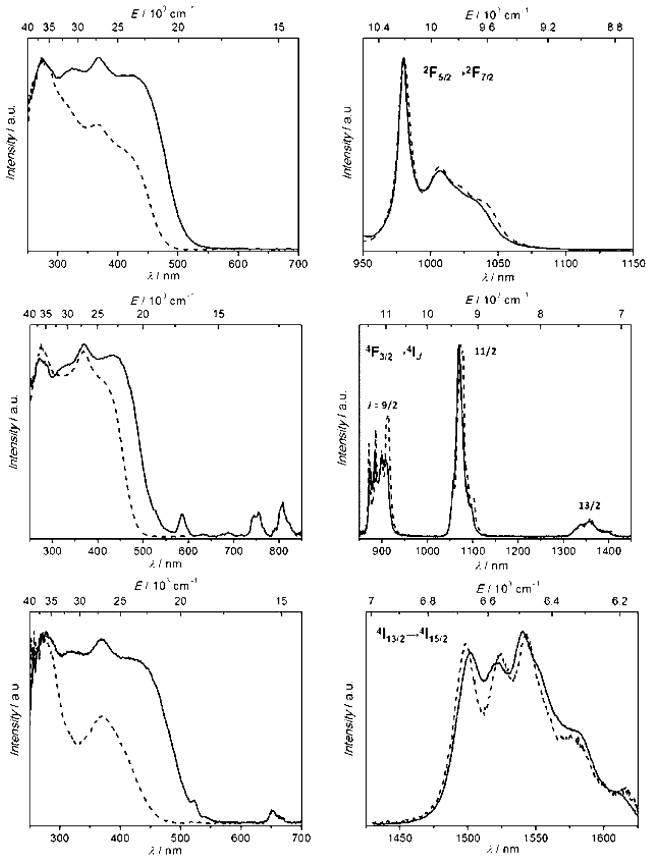

Figure 5. (**Left**) Corrected and normalized excitation and (**right**) emission spectra of Ln^{3+} MC complexes in solid state (λ_{ex} = 420 nm, solid traces) and methanol solution (1 mg/mL, λ_{ex} = 370 nm, dashed traces). (**Top**) $\mathbf{Yb^{3+}[Zn(II)MC_{quinHA}]}$, λ_{em} = 980 nm; (**Middle**) $\mathbf{Nd^{3+}[Zn(II)MC_{quinHA}]}$, λ_{em} = 1064 nm; (**Bottom**) $\mathbf{Er^{3+}[Zn(II)MC_{quinHA}]}$, λ_{em} = 1525 nm.

are dominated by ligand-centered broad-bands pointing toward efficient sensitization of lanthanide cations operating through the electronic structure of the chromophoric ligands. Excitation spectra of $\mathbf{Nd^{3+}[Zn(II)MC_{quinHA}]}$ and $\mathbf{Er^{3+}[Zn(II)MC_{quinHA}]}$ in the solid state exhibit characteristic sharp intraconfigurational f-f transitions with a lower relative intensity compared to the

dx.doi.org/10.1021/ja4113337 | J. Am. Chem. Soc. 2014, 136, 1526−1534

Table 1. Photophysical Parameters of $Ln^{3+}[Zn(II)MC_{quinHA}]$ and $Ln^{3+}[Zn(II)MC_{picHA}]$ Complexes (Ln^{3+} = Yb, Nd, Er) in Solid State and Methanol Solutions (1 mg/mL)[a]

compound	state/solvent	$\tau_{obs}/\mu s$[b]	q[c]	λ_{ex}/nm	Q^{L}_{Ln}/%
$Yb^{3+}[Zn(II)MC_{quinHA}]$	solid	47.8(4)		370	2.44(4)
	CH_3OH	14.88(1)	0		0.25(1)
	CD_3OD	150.7(2)			2.88(2)
$Yb^{3+}[Zn(II)MC_{picHA}]$	solid	34.5(1)		320	0.40(2)
	CH_3OH	12.1(1)	0		0.13(1)
	CD_3OD	133(1)			1.60(3)
$Nd^{3+}[Zn(II)MC_{quinHA}]$	solid	1.79(2)		370	1.13(4)
	CH_3OH	1.16(1)	0		0.38(1)
	CD_3OD	4.11(3)			1.35(1)
$Nd^{3+}[Zn(II)MC_{picHA}]$	solid	1.18(2)		320	0.40(1)
	CH_3OH	0.90(1)	0		0.22(2)
	CD_3OD	3.53(2)			0.98(1)
$Er^{3+}[Zn(II)MC_{quinHA}]$	solid	5.73(2)		370	$4.2(1)\cdot10^{-2}$
	CH_3OH	1.25(1)			$9.9(3)\cdot10^{-4}$
	CD_3OD	11.40(3)			$3.6(1)\cdot10^{-2}$

[a]Data for 298 K. Standard deviation (2σ) between parentheses; estimated relative errors: τ_{obs}, ±2%; Q^{L}_{Ln}, ±10%. [b]Under excitation at 355 nm. [c]The inner sphere hydration numbers were calculated according to the following equations: $q_{Yb} = 2 \times (k_{CH3OH} - k_{CD3OD} - 0.1)$ (in μs) and $q_{Nd} = 290 \times (k_{CH3OH} - k_{CD3OD}) - 0.4$ (in ns).[74,75]

broad-band ligand centered transitions. Excitation spectra of the MCs in diluted methanol solutions (0.1 mg/mL) match well the corresponding absorption spectra (Figure 5 vs Figures S7 and S8), while an expansion of the bands toward longer wavelengths is observed with increasing concentration (1 mg/mL) and for solid state samples. This observation may be a result of saturation effects and/or enhanced intermolecular interactions.[72,73]

Quantitative photophysical parameters are summarized in Tables 1 and S1. Experimental luminescence decays for all studied MCs are best fitted as monoexponential functions, reflecting the presence of only one emissive lanthanide-containing species. When going from solid state samples to methanol solutions, the observed luminescence lifetimes decrease by 1.5−5-fold, despite the fact that emission spectra are very similar by their bandwidths and crystal-field splitting, indicating that complexes remain intact/undissociated in solution. Nevertheless, τ_{obs} are comparable to the highest values reported to date for lanthanide complexes in protic solvents.[12,45] In deuterated methanol, luminescence lifetimes of 150.7(2), 4.11(3), and 11.40(3) μs were observed for Yb^{3+}, Nd^{3+} and Er^{3+} MCs, respectively. This represents a significant increase, by 3.5−10-fold, compared to samples in protonated solvent and a 2−3-fold increase relative to solid state samples. Calculations using phenomenological equations (which must be applied carefully, Table 1, footnote)[74,75] for $Yb^{3+}[Zn(II)MC_{quinHA}]$ and $Nd^{3+}[Zn(II)MC_{quinHA}]$ complexes are in line with the structural analysis and confirm that there are no solvent molecules bound to the lanthanide ion in the first coordination sphere. Therefore, such variations in luminescence lifetimes are the result of enhanced nonradiative deactivation through outer-sphere interactions with solvent molecules.

Under excitation into the charge-transfer band at 370 nm, luminescence quantum yields vary only slightly between solid state samples and solutions in deuterated methanol for $Yb^{3+}[Zn(II)MC_{quinHA}]$ (2.44 vs 2.88%), $Nd^{3+}[Zn(II)MC_{quinHA}]$ (1.13 vs 1.35%), and $Er^{3+}[Zn(II)MC_{quinHA}]$ ($[3.6-4.2]\bullet10^{-2}$%). The highest reported quantum yields for Yb^{3+}, Nd^{3+}, and Er^{3+}complexes containing C−H bonds are <3.8%, <0.42%, and <0.033%, respectively.[12,14,48] Values for Q^{L}_{Ln} measured here are the largest values reported to date for $Nd^{3+}[Zn(II)MC_{quinHA}]$ and $Er^{3+}[Zn(II)MC_{quinHA}]$. The values of Q^{L}_{Ln} decrease by 4−36-fold when measured in protonated solvent (CH_3OH) with the largest impact observed for $Er^{3+}[Zn(II)MC_{quinHA}]$. This difference can be explained by the influence of outer-sphere O−H vibrations; the Er^{3+} ion has the highest intrinsic probability among studied ions to be quenched nonradiatively by high-energy vibrations. Compared with the family of the previously published NIR-emitting MCs, $Ln^{3+}[Zn(II)MC_{picHA}]$ quantitative characteristics (luminescence lifetimes and quantum yields) in the solid state and methanol solutions of $Ln^{3+}[Zn(II)MC_{quinHA}]$ for both Nd^{3+} and Yb^{3+} derivatives are significantly improved (Table 1). Moreover, a replacement of picoline- with quinoline-hydroxamic acid allows extension of the absorption up to 450 nm.

In order to get additional quantitative information about energy transfer processes in lanthanide complexes, it is crucial to obtain the radiative lifetime (τ_{rad}), which equates to the lifetime in the absence of any nonradiative transitions, described by eq 1 where Q^{Yb}_{Yb} is the intrinsic quantum yield, and η_{sens} is the sensitization efficiency of the ligand.

$$Q^{L}_{Yb} = \eta_{sens} Q^{Yb}_{Yb} = \eta_{sens} \frac{\tau_{obs}}{\tau_{rad}} \quad (1)$$

Radiative lifetime is usually ignored by researchers; however, it is clear from eq 1 that finding ways to modulate this parameter can improve the intrinsic quantum yield, as τ_{rad} is inversely proportional to Q^{Yb}_{Yb}.[76] In the case of $Yb^{3+}[Zn(II)MC_{quinHA}]$ and $Er^{3+}[Zn(II)MC_{quinHA}]$, luminescence transitions terminate onto the ground level, so the absorption spectrum corresponding to the emission spectrum might be measured and used to calculate radiative lifetimes with the help of the modified Einstein's equation (eqs 2a-2b) where c is the speed of light in centimeters per second, n is refractive index (n_{CH3OH} = 1.329), N_A is Avogadro's number, J and J' are the quantum numbers for the ground and excited states, respectively, $\int \varepsilon(\tilde{\nu}) d\tilde{\nu}$ is the integrated spectrum of the f-f transition, and $\tilde{\nu}_m$ is the barycenter of the transition.

dx.doi.org/10.1021/ja4113337 | J. Am. Chem. Soc. 2014, 136, 1526−1534

$$\frac{1}{\tau_{rad}} = 2303 \times \frac{8\pi c n^2 \tilde{\nu}_m^{\ 2}(2J+1)}{N_A(2J'+1)} \int \varepsilon(\tilde{\nu})d\tilde{\nu} \quad (2a)$$

$$\tilde{\nu}_m = \frac{\int \tilde{\nu}\varepsilon(\tilde{\nu})d\tilde{\nu}}{\int \varepsilon(\tilde{\nu})d\tilde{\nu}} \quad (2b)$$

It is known that f-f transitions have very low molar absorption coefficients, and we only could succeed in measuring the absorption spectrum of the $^2F_{5/2} \leftarrow {}^2F_{7/2}$ transition in $\mathbf{Yb^{3+}[Zn(II)MC_{quinHA}]}$ (Figure S5). A value of τ_{rad} = 0.68(7)ms was found for $\mathbf{Yb^{3+}[Zn(II)MC_{quinHA}]}$, which is shorter than the radiative lifetimes reported for Yb^{3+}(diethylenetriaminepentaacetate)$^{2-}$ and Yb^{3+}(dipicolinate)$^{3-}$ complexes (1.2−1.3 ms)[77,78] or for Yb^{3+} with terphenyl-based ligands, ∼2 ms,[79] but close to the values found for Yb^{3+} complexes with benzoxazole-substituted 8-hydroxyquinolines (0.7−0.75 ms) which exhibit high quantum yields.[44] Using eq 1 and taking into account τ_{obs} and Q_{Ln}^{L} of $\mathbf{Yb^{3+}[Zn(II)MC_{quinHA}]}$ in methanol (Table 1), we have been able to obtain quite modest values of the intrinsic quantum yield, 2.2(3)%, and of the sensitization efficiency of the ligand, 12(3)%. The latter might be the result of the relatively long distance between the lanthanide cation and the quinHA chromophore. Nevertheless, in protic solvents the main path of energy loss remains the nonradiative deactivation through O−H vibrations.

One major advantage of Ln^{3+} based luminescent reporters, as mentioned above, is their excellent photostability. In order to compare the photostability of our system to the behavior of an organic fluorophore, $\mathbf{Yb^{3+}[Zn(II)MC_{quinHA}]}$, $\mathbf{Nd^{3+}[Zn(II)MC_{quinHA}]}$, and an organic cyanine dye (3,3′-diethylthiadicarbocyanine iodide) were irradiated at 400 or 610 nm, respectively, and luminescence intensity of the lanthanide signal (980 or 1064 nm) or corresponding organic emission (670 nm) bands were recorded over an extended period of time (t > 120 min). Over the course of this experiment, Yb^{3+} and Nd^{3+} luminescence intensity remained unchanged for the corresponding $\mathbf{Yb^{3+}[Zn(II)MC_{quinHA}]}$ and $\mathbf{Nd^{3+}[Zn(II)MC_{quinHA}]}$ complexes, whereas the NIR cyanine dye suffered from more than a 5-fold reduction in luminescence intensity over the same period of time (Figure S9). This result highlights the favorability of this and other luminescent Ln^{3+} based systems over de facto organic chromophores.

CONCLUSIONS

The goal of this work was to improve the photophysical properties of near-infrared emitting lanthanide-based metallacrowns in order to broaden the applicability of this class of compounds. In particular, we would like to demonstrate that the versatility of MC strategy allows shifting the excitation wavelength toward lower energy through appropriate design of the chromophore and enhancing the quantitative luminescence parameters without affecting the global MC structure.

We have reported here a series of second generation lanthanide "encapsulated sandwich" MC complexes with the general formula $Ln^{3+}[12\text{-}MC_{Zn(II),quinHA}\text{-}4]_2[24\text{-}MC_{Zn(II),quinHA}\text{-}8]$ ($\mathbf{Ln^{3+}[Zn(II)MC_{quinHA}]}$, Ln^{3+} = Y, Nd, Eu, Gd, Tb, Dy, Er, Yb) in which the MC framework is formed by the self-assembled organization of Zn^{2+} ions and a tetradentate chromophoric ligand based on quinaldichydroxamic acid (quinHA). In comparison to the previously published lanthanide-based MCs, the change of picoline hydroxamic acid (picHA) to quinHA did not lead to significant changes in the coordination of the zinc and lanthanide metal ions and to the general arrangement of the chromophoric moieties, allowing the system to fully benefit from the unique MC structure. Indeed, nonradiative deactivation originating from overtones vibrations often play a key role in the quenching of NIR-emitting lanthanide cations in complexes formed with organic chromophoric ligands that transfer energy to the luminescent ion. This type of quenching limits the photonic output of the complexes and their use in practical applications. The unique encapsulated sandwich metallacrown structure allows one to set lanthanide ions at a predetermined and relatively shielded position so that the closest C−H group is located at a fixed and constant ∼7 Å distance. Photophysical properties of $\mathbf{Ln^{3+}[Zn(II)MC_{quinHA}]}$ (Ln^{3+} = Yb^{3+}, Nd^{3+}, Er^{3+}) in the solid state confirmed the efficiency of this approach that imply long luminescence lifetimes and the highest quantum yield values reported to date for Nd^{3+} and Er^{3+}complexes with C−H bonds. In addition, unique to these particular MC complexes is the important absorption over a broad range of UV−visible wavelengths due to ligand-based transitions, including inter- and/or intraligand CT states. The latter may act as an efficient way of sensitization of NIR lanthanide-centered luminescence with high overall efficiency ($\varepsilon \times Q_{Ln}^{L}$) at 380 nm: 137/1584 for Yb^{3+}, 209/742 for Nd^{3+}, and 0.54/19.8 for Er^{3+} MCs in CH_3OH/CD_3OD solutions. However, a comparison of photophysical properties of $\mathbf{Ln^{3+}[Zn(II)MC_{quinHA}]}$ in the solid state and in solution indicates that the present MC structure still does not fully protect lanthanide ions from outer-sphere interactions with solvent molecules. Nevertheless, compared to the previously published $\mathbf{Ln^{3+}[Zn(II)MC_{picHA}]}$ quantitative characteristics (luminescence lifetimes and quantum yields) in solid state and methanol solutions of $\mathbf{Ln^{3+}[Zn(II)MC_{quinHA}]}$ for both Nd^{3+} and Yb^{3+} derivatives are significantly improved (Table 1). Moreover, a replacement of picoline- with quinoline-hydroxamic acid allows one to extend absorption up to 450 nm. Thus, the versatility of the MC strategy opens multiple possibilities to improve the current performance further and make the reported lanthanide MC complexes promising candidates for a number of luminescence applications.

ASSOCIATED CONTENT

Supporting Information

Supplementary tables, figures, and X-ray crystallographic parameters, including CIF files. This material is available free of charge via the Internet at http://pubs.acs.org.

AUTHOR INFORMATION

Corresponding Authors

stephane.petoud@inserm.fr.
vlpec@umich.edu.

Author Contributions

‡These authors contributed equally to this work.

Notes

The authors declare no competing financial interest.

ACKNOWLEDGMENTS

This research was supported in part by the National Science Foundation under grant CHE-1057331. E.R.T. is supported by the NIH Ruth L. Kirschstein National Research Service Award (GM102980-01A1) and the Burroughs Wellcome Fund

Collaborative Research Travel Grant. S.P. acknowledges support from Institut National de la Santé et de la Recherche Médicale (INSERM). The authors thank La Ligue contre le Cancer and La Région Centre for funding. The work in France was carried out in the frame of COST action (TD1004 and CM1006). This project has been funded by the European Community's Seventh Framework Programme (FP7/2007-2013) under grant agreement no. 611488.

REFERENCES

(1) Werts, M. H. V. *Sci. Prog.* **2005**, *88*, 101.
(2) Cable, M. L.; Levine, D. J.; Kirby, J. P.; Gray, H. B.; Ponce, A. *Adv. Inorg. Chem.* **2011**, *63*, 1.
(3) Hagan, A. K.; Zuchner, T. *Anal. Bioanal. Chem.* **2011**, *400*, 2847.
(4) Eliseeva, S. V.; Bünzli, J.-C. G. *New J. Chem.* **2011**, *35*, 1165.
(5) Bünzli, J.-C. G.; Eliseeva, S. V. *Chem. Sci.* **2013**, *4*, 1939.
(6) Butler, S. J.; Parker, D. *Chem. Soc. Rev.* **2013**, *42*, 1652.
(7) Verwilst, P.; Eliseeva, S. V.; Vander Elst, L.; Burtea, C.; Laurent, S.; Petoud, S.; Muller, R. N.; Parac-Vogt, T. N.; De Borggraeve, W. M. *Inorg. Chem.* **2012**, *51*, 6405.
(8) Montgomery, C. P.; Murray, B. S.; New, E. J.; Pal, R.; Parker, D. *Acc. Chem. Res.* **2009**, *42*, 925.
(9) Bünzli, J.-C. G. *Chem. Rev.* **2010**, *110*, 2729.
(10) Bonnet, C. S.; Buron, F.; Caille, F.; Shade, C. M.; Drahos, B.; Pellegatti, L.; Zhang, J.; Villette, S.; Helm, L.; Pichon, C.; Suzenet, F.; Petoud, S.; Toth, E. *Chem.—Eur. J.* **2012**, *18*, 1419.
(11) Caille, F.; Bonnet, C. S.; Buron, F.; Villette, S.; Helm, L.; Petoud, S.; Suzenet, F.; Toth, E. *Inorg. Chem.* **2012**, *51*, 2522.
(12) Eliseeva, S. V.; Bünzli, J.-C. G. *Chem. Soc. Rev.* **2010**, *39*, 189.
(13) Foucault-Collet, A.; Gogick, K. A.; White, K. A.; Villette, S.; Pallier, A.; Collet, G.; Kieda, C.; Li, T.; Geib, S. J.; Rosi, N. L.; Petoud, S. *Proc. Natl. Acad. Sci. U. S. A.* **2013**, *110*, 17199.
(14) Bünzli, J.-C. G.; Eliseeva, S. V. *J. Rare Earths* **2010**, *28*, 824.
(15) Bünzli, J.-C. G.; Comby, S.; Chauvin, A.-S.; Vandevyver, C. D. B. *J. Rare Earths* **2007**, *25*, 257.
(16) Suzuki, H. *J. Photochem. Photobiol., A* **2004**, *166*, 155.
(17) Zhang, Q. Y.; Huang, X. Y. *Prog. Mater. Sci.* **2010**, *55*, 353.
(18) van der Ende, B. M.; Aarts, L.; Meijerink, A. *Phys. Chem. Chem. Phys.* **2009**, *11*, 11081.
(19) Yuan, L.; Lin, W.; Zheng, K.; He, L.; Huang, W. *Chem. Soc. Rev.* **2013**, *42*, 622.
(20) Bünzli, J.-C. G.; Eliseeva, S. V. In *Comprehensive Inorganic Chemistry II*, 2nd ed.; Jan, R., Kenneth, P., Eds.; Elsevier: Amsterdam, 2013; p 339.
(21) Zhang, T.; Zhu, X.; Wong, W.-K.; Tam, H.-L.; Wong, W.-Y. *Chem.—Eur. J.* **2013**, *19*, 739.
(22) Wong, W.-K.; Zhu, X.; Wong, W.-Y. *Coord. Chem. Rev.* **2007**, *251*, 2386.
(23) Tsvirko, M. P.; Meshkova, S. B.; Venchikov, V. Y.; Topilova, Z. M.; Bol'shoi, D. V. *Opt. Spectrosc.* **2001**, *90*, 669.
(24) Zhang, J.; Shade, C. M.; Chengelis, D. A.; Petoud, S. *J. Am. Chem. Soc.* **2007**, *129*, 14834.
(25) Comby, S.; Gunnlaugsson, T. *ACS Nano* **2011**, *5*, 7184.
(26) Truman, L. K.; Comby, S.; Gunnlaugsson, T. *Angew. Chem., Int. Ed.* **2012**, *51*, 9624.
(27) Andolina, C. M.; Klemm, P. J.; Floyd, W. C.; Frechet, J. M. J.; Raymond, K. N. *Macromolecules* **2012**, *45*, 8982.
(28) Cross, J. P.; Lauz, M.; Badger, P. D.; Petoud, S. *J. Am. Chem. Soc.* **2004**, *126*, 16278.
(29) Branchi, B.; Ceroni, P.; Balzani, V.; Klärner, F.-G.; Vögtle, F. *Chem.—Eur. J.* **2010**, *16*, 6048.
(30) Eom, Y.; Ryu, J.; Bünzli, J.-C. G.; Baek, J.-B.; Kim, H. *Macromol. Res.* **2013**, *21*, 556.
(31) Pillai, Z. S.; Ceroni, P.; Kubeil, M.; Heldt, J.-M.; Stephan, H.; Bergamini, G. *Chem. - Asian J.* **2013**, *8*, 771.
(32) Molard, Y.; Labbé, C.; Cardin, J.; Cordier, S. *Adv. Funct. Mater.* **2013**, *23*, 4821.
(33) Brunet, E.; Jimenez, L.; de Victoria-Rodriguez, M.; Luu, V.; Muller, G.; Juanes, O.; Rodriguez-Ubis, J. C. *Microporous Mesoporous Mater.* **2013**, *169*, 222.
(34) Gu, Y.-J.; Yan, B. *Eur. J. Inorg. Chem.* **2013**, *2013*, 2963.
(35) Abdelhameed, R. M.; Carlos, L. D.; Silva, A. M. S.; Rocha, J. *Chem. Commun.* **2013**, *49*, 5019.
(36) Gong, H.-Y.; Rambo, B. M.; Nelson, C. A.; Lynch, V. M.; Zhu, X.; Sessler, J. L. *Chem. Commun.* **2012**, *48*, 10186.
(37) Decadt, R.; Van Hecke, K.; Depla, D.; Leus, K.; Weinberger, D.; Van Driessche, I.; Van Der Voort, P.; Van Deun, R. *Inorg. Chem.* **2012**, *51*, 11623.
(38) An, J.; Shade, C. M.; Chengelis-Czegan, D. A.; Petoud, S.; Rosi, N. L. *J. Am. Chem. Soc.* **2011**, *133*, 1220.
(39) Singaravadivel, S.; Babu, E.; Velayudham, M.; Lu, K.-L.; Rajagopal, S. *J. Organomet. Chem.* **2013**, *738*, 49.
(40) Singaravadivel, S.; Babu, E.; Velayudham, M.; Lu, K.-L.; Rajagopal, S. *Polyhedron* **2013**, *60*, 54.
(41) Yang, X.; Schipper, D.; Jones, R. A.; Lytwak, L. A.; Holliday, B. J.; Huang, S. *J. Am. Chem. Soc.* **2013**, *135*, 8468.
(42) Xu, H.-B.; Li, J.; Shi, L.-X.; Chen, Z.-N. *Dalton Trans.* **2011**, *40*, 5549.
(43) Xu, H.-B.; Zhong, Y.-T.; Zhang, W.-X.; Chen, Z.-N.; Chen, X.-M. *Dalton Trans.* **2010**, *39*, 5676.
(44) Shavaleev, N. M.; Scopelliti, R.; Gumy, F.; Bünzli, J.-C. G. *Inorg. Chem.* **2009**, *48*, 7937.
(45) Bünzli, J.-C. G.; Piguet, C. *Chem. Soc. Rev.* **2005**, *34*, 1048.
(46) Bredol, M.; Kynast, U.; Ronda, C. *Adv. Mater.* **1991**, *3*, 361.
(47) Malta, O. L.; Brito, H. F.; Menezes, J. F. S.; Gonçalves e Silva, F. R.; de Mello Donegá, C.; Alves, S., Jr. *Chem. Phys. Lett.* **1998**, *282*, 233.
(48) Comby, S.; Bünzli, J.-C. G. In *Handbook on the Physics and Chemistry of Rare Earths, Vol 37: Optical Spectroscopy*; Gschneidner, K. A., Bünzli, J.-C. G., Pecharsky, V. K., Eds.; Elsevier Science: Amsterdam, 2007.
(49) Hasegawa, Y.; Wada, Y.; Yanagida, S. *J. Photochem. Photobiol., C* **2004**, *5*, 183.
(50) Winkless, L.; Tan, R. H. C.; Zheng, Y.; Motevalli, M.; Wyatt, P. B.; Gillin, W. P. *Appl. Phys. Lett.* **2006**, *89*, 111115 DOI: 10.1063/1.2345909.
(51) Monguzzi, A.; Tubino, R.; Meinardi, F.; Biroli, A. O.; Pizzotti, M.; Demartin, F.; Quochi, F.; Cordella, F.; Loi, M. A. *Chem. Mater.* **2008**, *21*, 128.
(52) Hernández, I.; Tan, R. H. C.; Pearson, J. M.; Wyatt, P. B.; Gillin, W. P. *J. Phys. Chem. B* **2009**, *113*, 7474.
(53) Pizzoferrato, R.; Francini, R.; Pietrantoni, S.; Paolesse, R.; Mandoj, F.; Monguzzi, A.; Meinardi, F. *J. Phys. Chem. A* **2010**, *114*, 4163.
(54) Mezei, G.; Zaleski, C. M.; Pecoraro, V. L. *Chem. Rev.* **2007**, *107*, 4933.
(55) Grant, J. T.; Jankolovits, J.; Pecoraro, V. L. *Inorg. Chem.* **2012**, *51*, 8034.
(56) Seda, S. H.; Janczak, J.; Lisowski, J. *Inorg. Chem. Commun.* **2006**, *9*, 792.
(57) Stemmler, A. J.; Kampf, J. W.; Kirk, M. L.; Atasi, B. H.; Pecoraro, V. L. *Inorg. Chem.* **1999**, *38*, 2807.
(58) Boron, T. T.; Kampf, J. W.; Pecoraro, V. L. *Inorg. Chem.* **2010**, *49*, 9104.
(59) Cutland, A. D.; Malkani, R. G.; Kampf, J. W.; Pecoraro, V. L. *Angew. Chem., Int. Ed.* **2000**, *39*, 2689.
(60) Lim, C. S.; Jankolovits, J.; Zhao, P.; Kampf, J. W.; Pecoraro, V. L. *Inorg. Chem.* **2011**, *50*, 4832.
(61) Zaleski, C. M.; Lim, C. S.; Noord, A.; Kampf, J. W.; Pecoraro, V. L. *Inorg. Chem.* **2011**, *50*, 7707.
(62) Jankolovits, J.; Lim, C. S.; Kampf, J. W.; Pecoraro, V. L. *Z. Naturforsch., B: J. Chem. Sci.* **2010**, *65*, 263.
(63) Jankolovits, J.; Andolina, C. M.; Kampf, J. W.; Raymond, K. N.; Pecoraro, V. L. *Angew. Chem., Int. Ed.* **2011**, *50*, 9660.
(64) Reddy, A. S.; Kumar, M. S.; Reddy, G. R. *Tetrahedron Lett.* **2000**, *41*, 6285.

(65) Jankolovits, J.; Kampf, J. W.; Pecoraro, V. L. *Inorg. Chem.* **2013**, *52*, 5063.
(66) Eckstein, Z.; Lipczynska-Kochany, E.; Leszczynska, E. *Monatsh. Chem.* **1983**, *114*, 1009.
(67) Yin, Z.; Low, K.; Lye, P. *Synth. Commun.* **2005**, *35*, 2945.
(68) Bahnemann, D. W.; Kormann, C.; Hoffmann, M. R. *J. Phys. Chem.* **1987**, *91*, 3789.
(69) Kunkely, H.; Vogler, A. *J. Chem. Soc., Chem. Commun.* **1990**, 1204.
(70) Bird, B. D.; Day, P. *Chem. Commun.* **1967**, 741.
(71) D'Aléo, A.; Pointillart, F.; Ouahab, L.; Andraud, C.; Maury, O. *Coord. Chem. Rev.* **2012**, *256*, 1604.
(72) Donega, C. D. M.; Meijerink, A.; Blasse, G. *J. Lumin.* **1994**, *62*, 189.
(73) Ganapathi, M.; Eliseeva, S. V.; Brooks, N. R.; Soccol, D.; Fransaer, J.; Binnemans, K. *J. Mater. Chem.* **2012**, *22*, 5514.
(74) Beeby, A.; Clarkson, I. M.; Dickins, R. S.; Faulkner, S.; Parker, D.; Royle, L.; de Sousa, A. S.; Williams, J. A. G.; Woods, M. *J. Chem. Soc., Perkin Trans. 2* **1999**, 493.
(75) Faulkner, S.; Beeby, A.; Carrie, M. C.; Dadabhoy, A.; Kenwright, A. M.; Sammes, P. G. *Inorg. Chem. Commun.* **2001**, *4*, 187.
(76) Bünzli, J.-C. G.; Chauvin, A. S.; Kim, H. K.; Deiters, E.; Eliseeva, S. V. *Coord. Chem. Rev.* **2010**, *254*, 2623.
(77) Aebischer, A.; Gumy, F.; Bünzli, J.-C. G. *Phys. Chem. Chem. Phys.* **2009**, *11*, 1346.
(78) Werts, M. H. V.; Jukes, R. T. F.; Verhoeven, J. W. *Phys. Chem. Chem. Phys.* **2002**, *4*, 1542.
(79) Klink, S. I.; Hebbink, G. A.; Grave, L.; Peters, F. G. A.; Van Veggel, F.; Reinhoudt, D. N.; Hofstraat, J. W. *Eur. J. Org. Chem.* **2000**, 1923.